Selection for Function: From Chemically Synthesized Prototypes to 3D-Printed Microdevices

Felix Bachmann, Joshua Giltinan, Agnese Codutti, Stefan Klumpp, Metin Sitti, and Damien Faivre*

Magnetic microswimmers are promising devices for biomedical and environmental applications. Bacterium flagella-inspired magnetic microhelices with perpendicular magnetizations are currently considered standard for propulsion at low Reynolds numbers because of their well-understood dynamics and controllability. Deviations from this system have recently emerged: randomly shaped magnetic micropropellers with nonlinear swimming behaviors show promise in sensing, sorting, and directional control. The current progresses in 3D micro/nanoprinting allow the production of arbitrary 3D microstructures, increasing the accessible deterministic design space for complex micropropeller morphologies. Taking advantage of this, a shape is systematically reproduced that was formerly identified while screening randomly shaped propellers. Its nonlinear behavior, which is called frequency-induced reversal of swimming direction (FIRSD), allows a propeller to swim in opposing directions by only changing the applied rotating field's frequency. However, the identically shaped swimmers do not only display the above-mentioned swimming property but also exhibit a variety of swimming behaviors that are shown to arise from differences in their magnetic moment orientations. This underlines not only the role of shape in microswimmer behavior but also the importance of determining magnetic properties of future micropropellers that act as intelligent devices, as single-shape templates with different magnetic moments can be utilized for different operation modes.

Magnetic microswimmers are envisioned for a multitude of biomedical applications.[1–6] Most micropropellers have helical shapes, as they are inspired by both their rotating bacteria flagella[7–12] and historical macroscopic precursors.[13,14] Microfabrication methods, such as glancing angle deposition[7,15,16] and biotemplating,[17,18] produce helical shapes on the micro- or even nanoscale. When actuated by a homogeneous, rotating magnetic field, a magnetic moment fixed perpendicular to the helix axis allows for controlled actuation at the microscale with a linear relationship between rotation frequency and propulsion velocity of the propeller.[15,19,20] This design paradigm has proven to be a solid basis for further development of potential biomedical applications and the focus of research therefore moved toward functionalization of such helical micropropellers or slight deviations from this shape.[21]

However, helices with a magnetic moment nonperpendicular to the helical axis have also attracted interest: they are envisioned for sensing[22] or cargo transport.[23] In addition, we previously demonstrated new prospects for microswimmers

Dr. F. Bachmann, Dr. A. Codutti,[+] Dr. D. Faivre
Department of Biomaterials
Max Planck Institute of Colloids and Interfaces
Science Park Golm, 14424 Potsdam, Germany
E-mail: damien.faivre@mpikg.mpg.de

Dr. J. Giltinan, Prof. M. Sitti
Physical Intelligence Department
Max Planck Institute for Intelligent Systems
70569 Stuttgart, Germany

(iD) The ORCID identification number(s) for the author(s) of this article can be found under https://doi.org/10.1002/aisy.202000078.

[+]Present address: Biological Physics and Morphogenesis, Max Planck Institute for Dynamics and Self-Organization, Am Faßberg 17, 37077 Göttingen, Germany

Dr. A. Codutti, Prof. S. Klumpp
Department of Theory and Biosystems
Max Planck Institute of Colloids and Interfaces
Science Park Golm, 14424 Potsdam, Germany

Prof. S. Klumpp
Institute for the Dynamics of Complex Systems
University of Göttingen
Friedrich-Hund-Platz 1, 37077 Göttingen, Germany

Prof. M. Sitti
School of Medicine and School of Engineering
Koc University
34450 Istanbul, Turkey

Dr. D. Faivre
Aix-Marseille Université, CEA, CNRS, BIAM
13 108 Saint Paul lez Durance, France

deviating from helical shapes. From a pool of chemically synthesized randomly shaped magnetic microswimmers, we identified individuals with swimming capabilities exceeding those of propellers synthesized by most sophisticated and conventional solutions.[19,24] Theoretical as well as experimental studies demonstrated that these new sorts of devices exhibit a nonlinear velocity–frequency dependence that allows new control options.[25,26] Combined with progress in two-photon polymerization (3D printing at the microscale), we decided to use a selection-for-function approach[19,25] and reproduced a given shape in high amounts and with high precision. The idea is to utilize the vast range of different propeller shapes and behaviors that we find in our pool of chemically synthesized randomly shaped propellers and identify a specific propeller behavior that is of interest for future applications. Extracting the propeller shape is assumed to be the base for its behavior. Accordingly, 3D printing will enable new ways to access useful propeller shapes beyond the current helicoidal standard. Here, we thus exemplarily report the transfer of a selected propeller shape with nonlinear behavior (frequency-induced reversal of swimming direction [FIRSD][25]) via the 3D printing of a 4.5 μm-long propeller on a 1:1 scale. The influence of the magnetic moment orientation on the propeller velocity was tested experimentally and shows both that the precise determination of these properties is necessary to achieve the desired unique behavior, and on the other hand, that a single shape can act as a "smart" device sensitive in different areas tuned by the propeller's magnetic moment. In addition, numeric simulations of the printed propeller shape with varying magnetic moment orientations support this conclusion.

We expect that these results provide new insights into the potential of magnetic micropropellers with nonhelical shapes and nonlinear velocity–frequency dependency. This will improve the utilization of the available shape-magnetism design space of

micropropellers when it comes to magnetic actuation of matter at the microscale.

Randomly shaped magnetic particles from a chemical hydrothermal synthesis[19,24] can be a way to cheaply produce high numbers of microswimmers. We previously showed how such microswimmers can be used for the motion control of single propellers,[19,24,25] swimming aggregates,[27] and the formation of clusters with thousands of propellers.[28] In addition, these propellers can be the foundation for an experimental extraction approach, which we called "selection for function." Such selected functions can range from shapes that provide fast swimming speeds[19] to propeller shapes that allow two swimming modes with opposing movement directions.[25] For instance, the two swimming modes from the latter example can be accessed by setting certain external actuation frequencies (FIRSD). The underlying mechanism of such devices[25,26,29] provides the potential for these propellers to act as "smart microswimmers" that can be used for advanced swarm control[25] or sensing systems.[22] Thus, we chose here a propeller showing such a behavior as the starting point for the prototypical transfer of behavior from a chemically synthesized propeller to a designed and controlled fabricated 3D-printed microdevice. It is important to note that we therefore deviate from using highly symmetrical, well-defined shapes that are usually studied in both theoretical and experimental surveys but focus on a direct shape transfer that is not limited by predesign deliberations. This can be seen as the experimental complement to theoretical optimization studies to find new shapes outside the norm that can be utilized under the envisioned complex application environments.

Figure 1 shows the frequency-dependent propulsion velocity of the selected chemically synthesized propeller, actuated by an external magnetic field strength of 3 mT between 5 and 100 Hz in 5 Hz steps.[25] In addition, sequential optical microscopy images indicate the shape and rotation orientation of this
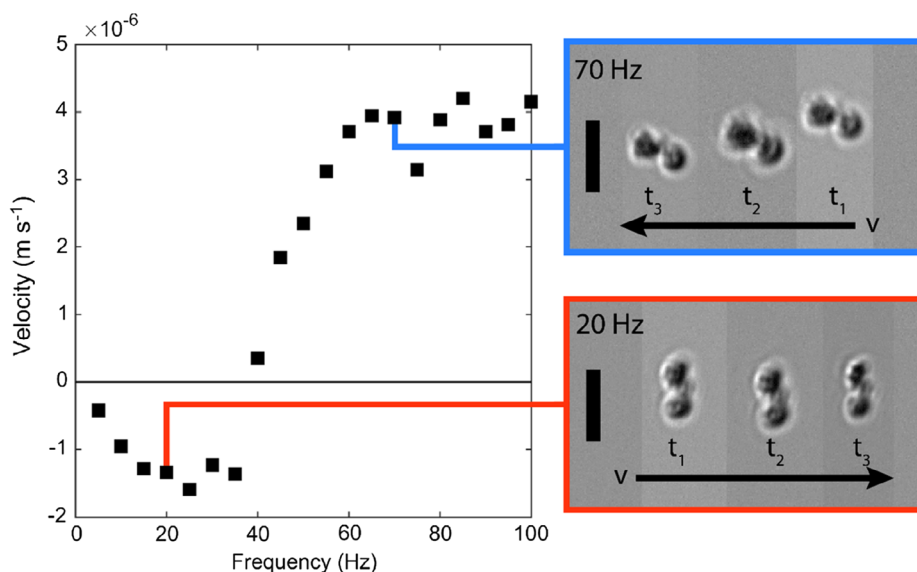
Figure 1. Selected propeller. The velocity–frequency graph of the original propeller selected from a pool of randomly shaped particles measured at an actuating magnetic field of 3 mT between 5 and 100 Hz in 5 Hz steps.[25] The propeller showed a reversal of swimming directions depending on the applied frequencies (FIRSD), which is shown by the microscope image sequence at 20 Hz and 70 Hz (relative time points are 0, 2, 4 s and 0, 1.2, 2.4 s, recorded at 50 frames per second). The scale bar is 5 μm.

propeller in the two accessible modes. At low frequencies (<35 Hz), the propeller has a negative velocity (swimming to the right) and rotates around its short axis. At high frequencies, the propeller rotates around its long axis and has a positive velocity (swims to the left). The maximum negative velocity is about $2\,\mu m\,s^{-1}$, the maximum positive velocity about $4\,\mu m\,s^{-1}$. The shown propeller is about $4.5\,\mu m$ on its longest dimension, has a maximum of about $2\,\mu m$ perpendicular to this direction, and roughly resembles a dumbbell shape with a bend thin link.

The optical images of the rotating selected propeller provide a view from all sides that is used for a back-projecting approach to reconstruct the 3D shape of the selected propeller.[25] The dimensions and general shape are well preserved in this reconstruction process; however, optical resolution limit, artifacts, and out-of-focus image generation hinder a perfect duplicate representation (comparison in **Figure 2**A,B). This reconstruction can be understood as a 3D voxel matrix and is the starting point of the reproduction process via 3D printing. This binary voxel matrix was converted to the stereolithography-format ".stl", and the structure was sliced at 200 nm intervals. The direct laser 3D lithography system Photonic Professional GT (Nanoscribe GmbH, Germany) uses this input data to print the complex propeller shape on a 1:1 scale, with a 200 nm printing resolution. Two versions were fabricated: one with the long axes of the propeller printed parallel (0°, Figure 2C) and one printed perpendicular (90°, Figure 2D) to the wafer surface. The propellers were subsequently coated with 100 nm nickel, which fixed a magnetic moment to the shape, with 100 nm titanium as protection layer. A hydrophobic monolayer of trichloro(1,1,2,2 H-perfluorooctyl) silane (Sigma Aldrich) was deposited by vapor to prevent the propellers from adhering to the capillary in which they were investigated. In Figure 2, the underlying 3D model (A, E, F) as well as scanning electron microscope (C, D) and optical microscope images (G, H) of the propeller are shown to illustrate the effective transfer of the selected shape on a 1:1 scale.

The magnetic properties of magnetic microswimmers are known not only to influence the regime of propulsion (via the actuating magnetic field strength and frequency) but in addition alter the frequency–velocity relationship of a magnetic
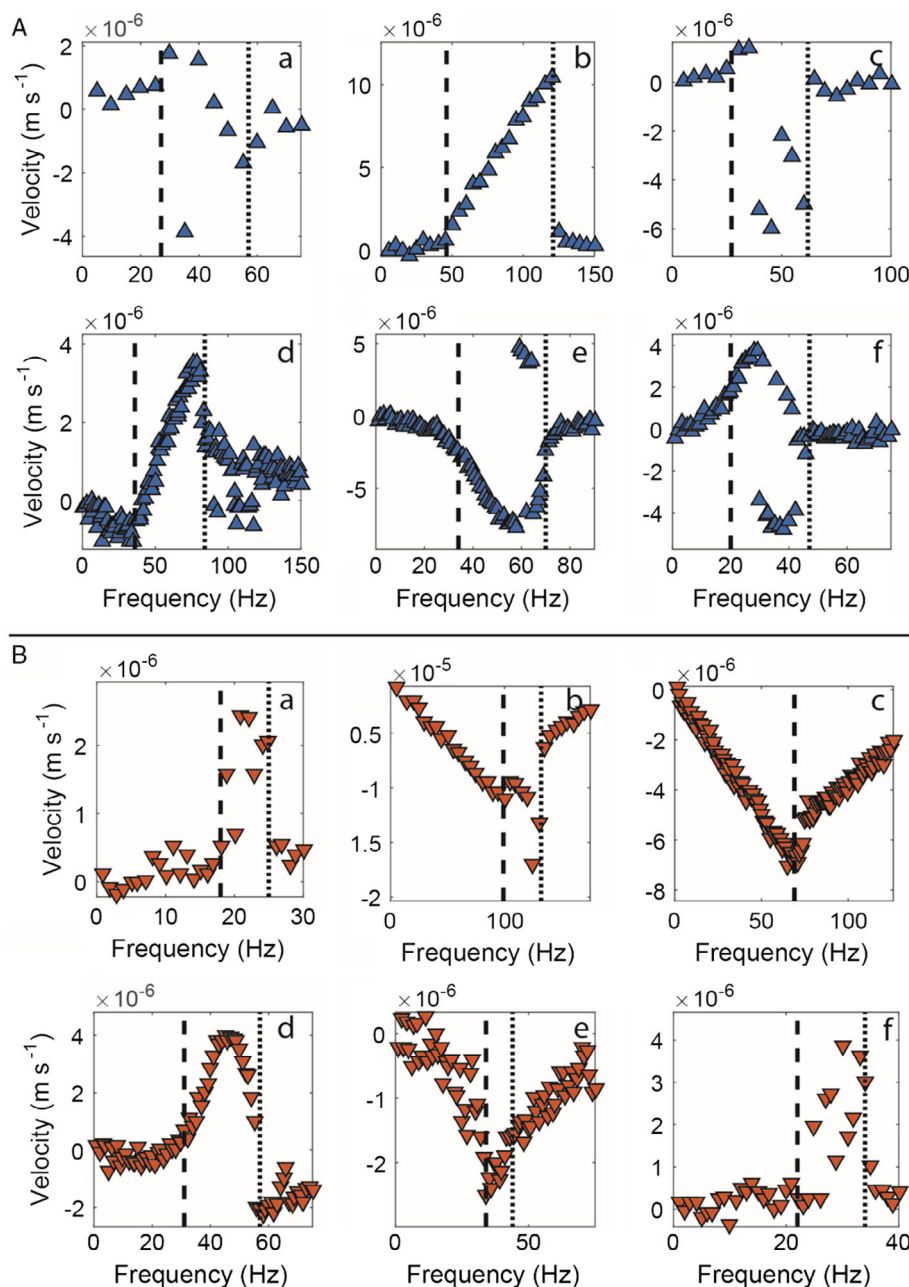
micropropeller.[25,26,30] Therefore, we initially assumed that printing the same propeller shape in different directions (0° and 90°) would lead to two different magnetization directions during the coating process and consequently to two different swimming behaviors. Accordingly, we tested the general swimming characteristics of few items per group. The propellers were actuated in single propeller measurements in bulk fluid with driving field strengths and measured frequencies adjusted for each run to capture the essential characteristic of each propeller (details in Supporting Information). **Figure 3** shows six examples of both groups of propellers (0° propellers: blue upward-pointing triangles, 90° propellers: red downward-pointing triangles). There are three main observations: 1) Some propellers show the expected behavior, similar to the initially selected propeller (Figure 1). 2) However, a larger space of different swimming behaviors is observed. 3) There is no clear consistency in behavior within each of the two propeller groups.

At least six of the shown propellers exhibit some form of FIRSD and therefore express the desired behavior, with propellers A/d and B/d in Figure 3 showing a good agreement in maximum negative and positive propeller velocities. However, no overall uniform behavior was observed with regard to the details of the frequency–velocity relationship, frequency and velocity range. An explanation for these points can be found in different magnetic moment orientations and magnitudes. The magnitude of magnetic moments scales the frequency regime of the swimming characteristics. Generally, these characteristics can be divided by two special frequencies into three regimes: a nearly linear tumbling regime, a typically nonlinear wobbling regime (where solution branching can occur[25,26,31]), and a so-called step-out regime. These frequencies are indicated in Figure 3 by dashed and dotted lines, respectively. Using a cylindrical approximation[29] for the rotational friction coefficient of the propeller shape, it is possible to estimate the magnitude of the magnetic moment (c.f. Supporting Information). The according values are shown in **Table 1** next to the used characteristic frequencies and applied external magnetic field strengths.

A plausible explanation for the rather different swimming behaviors relies on the differences in magnetic properties.[26,30,31]
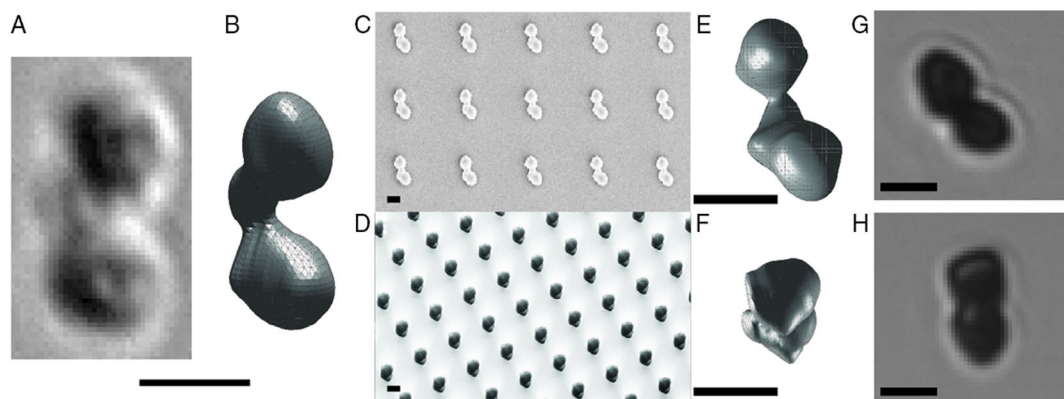
Figure 2. 3D-printed propellers. Optical microscopy images of a A) chemically synthesized propeller were used to reconstruct its 3D shape. This provides the B) template for 3D printing using the two-photon lithography technique. SEM images of the printed C) 0° and D) 90° propellers. E,F) Respective reconstructed 3D shapes orientated like the propellers in the SEM images. G,H) Respective optical microscope images of the printed propellers lying flat on a surface. All scale bars are 2 µm.

**ADVANCED
SCIENCE NEWS**

www.advancedsciencenews.com

**ADVANCED
INTELLIGENT
SYSTEMS**
Open Access

www.advintellsyst.com

Figure 3. Individual 3D-printed propeller measurements. The velocity–frequency graph of A) six 0° propellers (blue upward-pointing triangles) and B) six 90° propellers (red downward-pointing triangles) individually. The dashed line corresponds to f_{tw}, separating the tumbling and wobbling regime and the dotted line to f_{so}, separating the wobbling from the step-out regime (propeller B/c was not measured up to f_{so}). The values of these characteristic frequencies are approximations based on the propeller velocity and rotation behavior and are shown in Table 1, as they are used to estimate the respective magnetic moments.

To systematically study the effect of a change of magnetic moment orientation for a constant shape, a bead-based approximation of the propeller shape (inset **Figure 4**) was used to numerically solve the magnetic–hydrodynamic torque balance and calculate propeller velocity–frequency dependences.[30] The magnetic field strength (B_0) and the magnetic moment magnitude (m_0) were set constant ($B_0 = 1\,\text{mT}$ and $m_0 = 1 \times 10^{-14}\,\text{Am}^2$) throughout all calculations, to only detect the influence of the

magnetic moment orientation (varied spherically for with polar angle between 0° and 180° and azimuthal angle between −180° and 180°, as shown in the inset in Figure 4).

The velocity–frequency characteristics of a magnetic micropropeller scale with the strength of the actuating magnetic field B as well as with the magnitude of the magnetic moment m (see Supporting Information for more details). To compare experimental measurements of individual propellers (Figure 3)

Table 1. Magnetic fields and moments for individual measurements.

Exp.	A/a	A/b	A/c	A/d	A/e	A/f	B/a	B/b	B/c	B/d	B/e	B/f
B [mT]	1	1	1	0.5	0.5	0.5	2	1	3	0.5	0.5	3
f_{tw} [Hz]	27	46	27	36	34	20	18	99	69	31	34	22
f_{so} [Hz]	57	121	62	82	70	47	25	132	135[a]	57	44	34
m [10^{-14} Am^2]	2.17	4.23	2.28	6.04	5.47	3.40	0.61	6.54	1.78	4.63	4.44	0.51

[a]estimated value from cylindrical approximation fit, as the measurement was interrupted before f_{so} was reached.
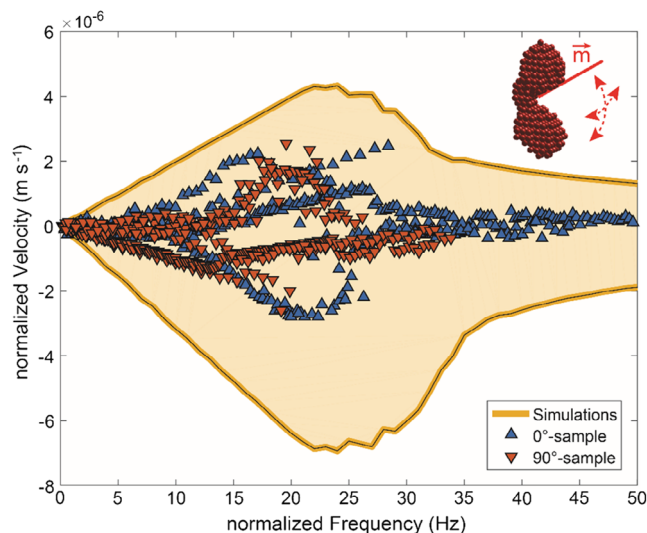
Figure 4. Variety of behaviors. Velocity measurements as a function of the applied field frequency for 0° (blue upward-pointing triangles) and 90° propellers (red downward-pointing triangles). All graphs are normalized on the magnetic field strength in $B_0 = 1$ mT and on their respective estimated magnetic moments in $m_0 = 1 \times 10^{-14}$ Am^2 (for the respective fields and moments of the individual measurements, see Table S1, Supporting Information). The yellow background reflects the possibilities calculated with numerical simulations by varying the magnetic moment orientation (schematically shown as the inset), with $B_0 = 1$ mT and $m_0 = 1 \times 10^{-14}$ Am^2.

that were carried out at different magnetic field strengths B and possess different magnetic moment magnitudes m (see Table 1), it is necessary to scale these graphs. Therefore, the experimental measurements (Figure 3) were normalized (division of velocities and frequencies by a factor of $(B \cdot m)/(B_0 \cdot m_0)$) on these values as well, using the magnetic field and moments from Table 1. This is possible, as the features (characteristic frequencies) and velocities of magnetic micropropellers scale linearly, with both the applied field strength and the magnetic moment magnitude.[25,32] Figure 4 shows these normalized experimental data (0° propellers: blue upward-pointing triangles, 90° propellers: red downward-pointing triangles). Although the individual graphs in Figure 3 show a variety of behaviors with a wide range of characteristic frequencies, the normalized graphs only cover a defined area in the frequency–velocity space (Figure 4). The simulations gave an according velocity–frequency graph for each

chosen magnetic moment orientation. Combining the results of these individual graphs results in the yellow background shown in Figure 4, with the yellow outlines giving the maximum and minimum velocities at the respective frequency. A qualitative agreement with the experimental data (shape of the covered area) is obtained; however, the numerical simulations are not quantitatively fitting. Possible reasons encompass 1) the used approximation of the propeller shape with beads;[30,33] 2) the number of experimentally measured propellers (twelve) which is too restricted and does not reflect the full spectrum of magnetic moment orientations; and 3) the 3D-printed geometries deviating from their 3D model, which results in a discrepancy in shape between experiments and simulations. Yet, a variation in magnetic moment orientation can explain the variance in the experimental results and, at the same time, illustrates the importance that lies in the exact determination of magnetic properties.

Although the focus here was in particular on the replication of the selected FIRSD behavior, it is important not to neglect the basic microswimmer property for operating at the microscale, which is propulsion speed. The dimensionless velocity $U = 1000 \times v/(f \times L)$, with the propulsion velocity v, the actuation frequency f, and the characteristic propeller length L serving as comparable measures. Recently, a shape/magnetization combination found theoretically with a genetic search algorithm for the optimal propulsion speed showed values of $U = 246$.[31] Our experimentally measured propellers had up to $U \approx 30$, whereas our simulation showed potential up to $U \approx 70$; hence, both values are way below the theoretical optimum. However, compared with other experimentally studied, helicoidally shaped propellers, they are well inside a practical regime (Zhang et al.:[11] $U = 20$; Li et al.:[34] $U = 30$; Gao et al.:[17] $U = 60$; and Ghosh and Fischer:[7] $U = 130$).

Overall, it was possible to reproduce a propeller shape via 3D printing that previously showed promising swimming characteristics (FIRSD) in a pool of randomly shaped propellers. Already among a small size of test 3D-printed propellers, the original behavior could at least qualitatively be reproduced in some cases. However, a wide range of the further behaviors was found, indicating that a precise tuning of the magnetic properties might play a predominant role compared with small details in shape. This is supported by numeric simulations of the used shape with varying magnetic moment orientations. A second experimental selection step with a pool of now 3D-printed propellers (filtering out the desired behavior) could give more uniform behaviors.[25] To not rely on such measures that relate to additional cost and time, the prototypical transfer process shown here can still be improved. There are several error-prone steps on the way from the originally selected propeller to its mass-produced 3D-printed equivalents. 1) 3D reconstruction: The quality of images taken for the 3D reconstruction algorithm[25] is limited by the optical resolution limit (several hundred nm, parts of the propeller being out of the focal plane), time resolution, number of images taken, and Brownian motion. The algorithm itself and filters try to counteract some of these artifacts; however, the reconstruction is only an acceptable representation of the real propeller (see Figure 2A,B). 2) 3D printing: The resolution of the printing process is, even with the most recent advances in 3D lithography, limited to about 5 % of the propeller size. This limits the amount

of details that can be incorporated. However, most other microswimmers that are currently produced via 3D printing are about one order of magnitude larger (>50 µm) than our prototype here (4.5 µm). 3) Magnetic properties: Coating the 3D-printed propellers with magnetic material in a vapor deposition process step is a simple and fast way to provide the propellers with a magnetic moment. This layer alters the propeller shape slightly. In addition, the magnetic material is often prone to oxidation, potentially altering the magnetic properties. Finally, as our measurements have shown, the magnetic moment orientation and strength vary between individual printed propellers. This is a general problem with this fabrication technique that is often neglected by only focusing on working examples (selection bias) or missing detailed measurements of the frequency–velocity relationship (distinction only between swimming and nonswimming). A potential alternative in determining magnetic properties could be incorporating magnetic beads in the printing resin, not relying on magnetic material deposition from the outside. First successes with this approach have already been achieved[35,36] but is still difficult for the needed precision.

Magnetic microswimmers have been proposed for biomedical and environmental applications of microscale robotics. On the way to realizing the envisioned applications, the propeller designs will become more nonintuitive as the required tasks that microdevices perform become more complex. Therefore, on the one hand, it is necessary to be able to produce complex shapes and on the other hand, to understand the interaction between these shapes and their magnetic and hydrodynamic characteristics. We replicated a previously selected propeller shape and behavior via 3D printing. A variety of further behaviors and velocity–frequency dependencies were measured, indicating different magnetic properties of the propellers with identical shapes. This influence was illustrated by showing the behavior space of a single shape with varying magnetic moment orientations via numeric simulations. These findings highlight that further development in 3D printing will be necessary before the potential of magnetic microswimmers can be fully utilized. This especially refers to new ways to control the magnetic properties of printed structures (e.g., including magnetic nanoparticles in certain parts of the resist[35,36] or local systems of magnetic multilayers that can provide directed magnetization[37]). Achieving this will open new doors for design and application of magnetic micropropellers as smart microdevices.

Supporting Information

Supporting Information is available from the Wiley Online Library or from the author.

Acknowledgements

Conflict of Interest

The authors declare no conflict of interest.

[1] H. Ceylan, J. Giltinan, K. Kozielski, M. Sitti, *Lab Chip* **2017**, *17*, 1705.
[2] M. Sitti, H. Ceylan, W. Hu, J. Giltinan, M. Turan, S. Yim, E. Diller, *Proc. IEEE* **2015**, *103*, 205.
[3] F. Qiu, B. J. Nelson, *Engineering* **2015**, *1*, 021.
[4] K. Bente, A. Codutti, F. Bachmann, D. Faivre, *Small* **2018**, *14*, 1704374.
[5] S. Klumpp, C. T. Lefèvre, M. Bennet, D. Faivre, *Phys. Rep.* **2019**, *789*, 1.
[6] J. Li, B. E. F. De Ávila, W. Gao, L. Zhang, J. Wang, *Sci. Robot.* **2017**, *2*, 1.
[7] A. Ghosh, P. Fischer, *Nano* **2009**, *7*.
[8] S. Tottori, L. Zhang, F. Qiu, K. K. Krawczyk, A. Franco-Obregōn, B. J. Nelson, *Adv. Mater.* **2012**, *24*, 811.
[9] R. Mhanna, F. Qiu, L. Zhang, Y. Ding, K. Sugihara, M. Zenobi-Wong, B. J. Nelson, *Small* **2014**, *10*, 1953.
[10] F. Qiu, R. Mhanna, L. Zhang, Y. Ding, S. Fujita, B. J. Nelson, *Sensors Actuators, B Chem.* **2014**, *196*, 676.
[11] L. Zhang, J. J. Abbott, L. Dong, K. E. Peyer, B. E. Kratochvil, H. Zhang, C. Bergeles, B. J. Nelson, *Nano Lett.* **2009**, *9*, 3663.
[12] H. C. Berg, R. A. Anderson, *Nature* **1973**, *245*, 380.
[13] K. Ishiyama, M. Sendoh, K. I. Arai, *J. Magn. Magn. Mater.* **2002**, *242–245*, 41.
[14] T. Honda, K. I. Arai, K. Ishiyama, *IEEE Trans. Magn.* **1996**, *32*, 5085.
[15] D. Schamel, M. Pfeifer, J. G. Gibbs, B. Miksch, A. G. Mark, P. Fischer, *J. Am. Chem. Soc.* **2013**, *135*, 12353.
[16] D. Schamel, A. G. Mark, J. G. Gibbs, C. Miksch, K. I. Morozov, A. M. Leshansky, P. Fischer, *ACS Nano* **2014**, *8*, 8794.
[17] W. Gao, X. Feng, A. Pei, C. R. Kane, R. Tam, C. Hennessy, J. Wang, *Nano Lett.* **2014**, *14*, 305.
[18] X. Yan, Q. Zhou, J. Yu, T. Xu, Y. Deng, T. Tang, Q. Feng, L. Bian, Y. Zhang, A. Ferreira, L. Zhang, *Adv. Funct. Mater.* **2015**, *25*, 5333.
[19] P. J. Vach, N. Brun, M. Bennet, L. Bertinetti, M. Widdrat, J. Baumgartner, S. Klumpp, P. Fratzl, D. Faivre, *Nano Lett.* **2013**, *13*, 5373.
[20] A. Cebers, M. Ozols, *Phys. Rev. E – Stat. Nonlinear, Soft Matter Phys.* **2006**, *73*, 1.
[21] C. Xin, L. Yang, J. Li, Y. Hu, D. Qian, S. Fan, K. Hu, Z. Cai, H. Wu, D. Wang, D. Wu, J. Chu, *Adv. Mater.* **2019**, *31*, 1808226.
[22] A. Ghosh, D. Dasgupta, M. Pal, K. I. Morozov, A. M. Leshansky, A. Ghosh, *Adv. Funct. Mater.* **2018**, *28*, 1.
[23] A. Barbot, D. Decanini, G. Hwang, *Sci. Rep.* **2016**, *6*, 1.
[24] P. J. Vach, P. Fratzl, S. Klumpp, D. Faivre, *Nano Lett.* **2015**, *15*, 7064.
[25] F. Bachmann, K. Bente, A. Codutti, D. Faivre, *Phys. Rev. Appl.* **2019**, *11*, 34039.
[26] K. I. Morozov, Y. Mirzae, O. Kenneth, A. M. Leshansky, *Phys. Rev. Fluids* **2017**, *2*, 1.
[27] P. J. Vach, D. Faivre, *Sci. Rep.* **2015**, *5*, 1.
[28] P. J. Vach, D. Walker, P. Fischer, P. Fratzl, D. Faivre, *J. Phys. D. Appl. Phys.* **2017**, *50*, 1.
[29] A. Ghosh, P. Mandal, S. Karmakar, A. Ghosh, *Phys. Chem. Chem. Phys.* **2013**, *15*, 10817.
[30] A. Codutti, F. Bachmann, D. Faivre, S. Klumpp, *Front. Robot. AI* **2018**, *5*, 1.

[31] Y. Mirzae, O. Dubrovski, O. Kenneth, K. I. Morozov, A. M. Leshansky, *Sci. Robot.* **2018**, *3*, eaas8713.

[32] P. J. Vach, S. Klumpp, D. Faivre, *J. Phys. D. Appl. Phys.* **2015**, *49*, 65003.

[33] B. Carrasco, J. G. De La Torre, *Biophys. J.* **1999**, *76*, 3044.

[34] J. Li, S. Sattayasamitsathit, R. Dong, W. Gao, R. Tam, X. Feng, S. Ai, J. Wang, *Nanoscale* **2014**, *6*, 9415.

[35] H. Ceylan, I. C. Yasa, O. Yasa, A. F. Tabak, J. Giltinan, M. Sitti, *ACS Nano* **2019**, *13*, 3353.

[36] H. W. Huang, M. S. Sakar, A. J. Petruska, S. Pané, B. J. Nelson, *Nat. Commun.* **2016**, *7*, 1.

[37] L. Baraban, D. Makarov, R. Streubel, I. Mönch, D. Grimm, S. Sanchez, O. G. Schmidt, *ACS Nano* **2012**, *6*, 3383.

2000078 (7 of 7)